

# **Mathematical modeling and simulation of the chemotactic movement of neutrophils in inflammatory environments**

**Masterarbeit**

zur Erlangung des Grades

**Master of Science (M.Sc.)**

**im Studiengang Computational and Applied  
Mathematics**

am Department Mathematik der  
Friedrich-Alexander-Universität Erlangen-Nürnberg

vorgelegt am 28.09.2022

von **Lorenzo Tapia Schulze**

Betreuerin: PD Dr. Maria Neuss-Radu



Friedrich-Alexander-Universität  
Naturwissenschaftliche Fakultät



---

*To Stefano.*

## Contents

<b>1</b>	<b>Introduction</b>	<b>1</b>
<b>2</b>	<b>Biomedical background</b>	<b>2</b>
2.1	Polymorphonuclear leukocytes (PMNs) . . . . .	2
2.2	Chemoattractant and chemotactic movement . . . . .	3
2.3	Chemoattractant-derived production of reactive oxygen species . . . . .	3
2.4	Experimental setup . . . . .	6
<b>3</b>	<b>Mathematical modeling</b>	<b>7</b>
3.1	Metabolic network for ROS . . . . .	7
3.2	Mathematical model . . . . .	7
<b>4</b>	<b>Numerical results</b>	<b>12</b>
4.1	Simulation with given chemoattractant concentration . . . . .	14
4.2	Simulation with variable chemoattractant concentration . . . . .	18
<b>5</b>	<b>Conclusion</b>	<b>24</b>
	<b>Literature</b>	<b>25</b>

# 1 Introduction

The human immune system has the important task to protect our body against harmful agents. In case that any pathogen enters our body, the immune system relies mostly on particular white blood cells called neutrophils. They play a fundamental role after tissue inflammation, due to their ability to imprison and degrade those pathogens.

Neutrophils identify the correct path towards the inflammatory site while they follow increasing concentrations of inflammatory cytokines; this phenomenon is called chemotaxis. To accomplish their defensive task, neutrophils produce high amounts of cytotoxic molecules that require oxygen consumption, called reactive oxygen species (ROS). This process was denoted as the respiration burst and it was described about ninety years ago [1]. Later research on neutrophil activity have confirmed that ROS production is required in a variety of intracellular processes that trigger important functional responses in neutrophils, such as cell motility [2].

Mathematical models for chemotaxis have been developed since the 1970s, starting with E. Keller and L. Segel [3]. From that year on, several chemotactic processes were described using the model in [3], e.g., in the work of A. Kettemann and M. Neuss-Radu [4] and M. Gabel [5]. Furthermore, mathematical analysis of biochemical processes started at the beginning of the 20th century, when a mathematical model describing enzyme kinetics was suggested by L. Michaelis and M. Menten in 1913 [6]. Their model might be the most famous when it comes to enzymatic reactions. It is still used to describe a huge variety of biochemical processes due to their dependence on enzymatic activity, as the respiration burst also does [7].

In the present work, we derive a mathematical model describing the chemotactic movement of neutrophils in inflammatory environments under the influence of the chemoattractant, and we include both the respiratory burst and ROS influence upon the motility of neutrophils. Thus, the chemotactic sensitivity is not a constant as in [3] but a function depending on ROS. Other mathematical models that include a non-constant chemotactic sensitivity, which depends on the cells or the chemoattractant can be found in [4, 5, 8].

This thesis was elaborated in the framework of a joint collaboration with the group of Dr. Michael Gruber (University Medical Center Regensburg), where experimental investigations on neutrophil activity were performed [9]. The final goal of this thesis is to analyze qualitatively the influence that ROS have on the cells' chemotactic movement.

The text is organized as follows: In Section 2, we give a brief biological background. The chemotaxis and the respiration burst in the context of neutrophil activity is described. In Section 3 the mathematical model is formulated. We present the PDE system together with the boundary conditions and the initial values that complete our model. In Section 4 we include the results from the numerical simulations and discuss about qualitative aspects. Finally, in Section 5, we present an outlook of this work together with possible upgrades of the model.

## 2 Biomedical background

### 2.1 Polymorphonuclear leukocytes (PMNs)

The human immune system relies strongly on the activity of *polymorphonuclear cells*. These white blood cells are also called *granulocytes* and we can classify them into different subcategories, e.g., neutrophils, who are also referred as *polymorphonuclear leukocytes (PMNs)*. The term *polymorphonuclear* comes from the shape of their nucleus; it exhibits several lobes (see Fig. 1). Neutrophils are responsible for the elimination of pathogens as bacteria, fungi, etc., although they also might lead to autoimmune diseases if the control mechanisms of their defensive activity does not work properly (e.g., see [10, 11]).

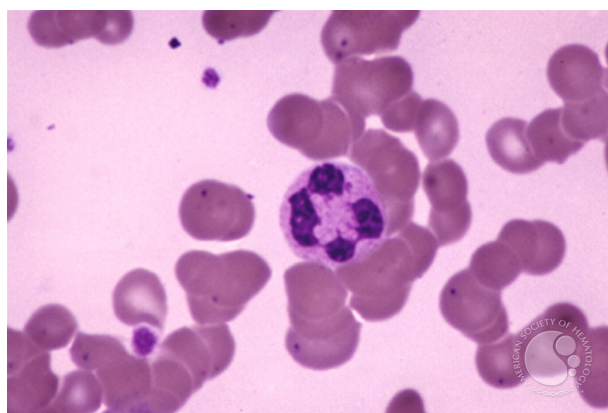


Figure 1: A neutrophil with its lobed nucleus.<sup>1</sup>

In a healthy body, neutrophils circulate freely within the blood or reside inside the bone marrow. After some part of the body becomes infected, an inflammatory response is sent from the infection site. That response consists of releasing biochemical substances into the blood, *inflammatory cytokines*, whose purpose is to attract neutrophils towards the infection site. Cytokines induce the activation of particular adhesion molecules in the endothelial cells and in neutrophils, such that these can adhere to the endothelium and start rolling in the direction of infection. Neutrophils move by sensing high concentrations of these cytokines [12]. This phenomenon, the movement of a body towards a concentration gradient, is called *chemotaxis*; the substance which triggers it, *chemoattractant* (e.g., see [10, 13]).

While the cells actively move, they produce high concentrations of *reactive oxygen species (ROS)*. Those molecules are radicals with a wide-ranging field of function. In the context of PMNs, their task is to damage pathogens. The excessive generation of ROS as a defense mechanism was named *respiration burst* or *oxidative burst* [10, 13].

After chemotaxis, neutrophils arrive to the infection site and start attacking the pathogen. The most famous mechanism is *phagocytosis*, which consists of engulfing

---

<sup>1</sup>This image was originally published in ASH Image Bank. Peter Maslak. Neutrophils - 1. ASH Image Bank. 2002; #00001592. © the American Society of Hematology.

and keeping it insides phagosomes, where it is supposed to be killed. Another mechanism is releasing the granuli containing ROS to the extracellular medium, such that they damage the pathogens severely. Recently, a new mechanism has been described: neutrophils attempt to trap the pathogen using a structure called *extracellular traps* (*ETs*) [10]. This mechanism is called *NETosis* (from *neutrophil extracellular trap*) and usually ends in cell death. However, it is still an open research question which mechanism to counteract pathogens is dominant in which situation [14].

It is known that the intensity of neutrophil activity usually differs from cell to cell. They can be stimulated previously by e.g. chemokines [13], and even environmental factors are relevant to their activity and to chemotaxis [10]. Those factors are out of the scope of this investigation.

## 2.2 Chemoattractant and chemotactic movement

In general, there are different kinds of chemoattractants such as lipids, cytokines and peptides. Chemoattractants are usually produced naturally by bacteria or by human cells, as a response to infection. A common chemoattractant for the chemotaxis of neutrophils is *N-formyl-methionyl-leucyl-phenylalanine* (*fMLP* or *fMLF*), which is produced by degradation of bacterial components [13, 15].

Chemoattractants bind to membrane-bound receptors on the neutrophil membrane [16]. These receptors belongs to the family of *guanine nucleotide-binding protein (G protein)-coupled receptors* (*GPCRs*) [17]. The receptor associated to fMLP is called *formyl peptide receptor* (*FPR*); in humans it was the first one to be cloned. If the activation of neutrophils persist in time, FPRs react to mitochondrial damage signals and thus induce a longer killing activity [13, 18].

Under the presence of fMLP, the cell's response is the chemotaxis towards higher concentration of the chemoattractant and a reaction cascade that triggers the oxidative burst [12]. Interestingly, the required amount of fMLP for ROS production is almost 50 to 100 times higher than only for chemotaxis [15]. In general, each chemoattractant elicits a specific response in terms of intensity. Furthermore, the levels of preference differ. In case of fMLP, the attraction is highly predominant [7].

The reaction cascade which induces the oxidative burst comprises different stages [13]. An important one is the activation of several proteins called *kinases*, e.g., mitogen-activated protein kinases (MAPK), protein kinases C (PKC) and protein kinases B (Akt). Those kinases are responsible of the partial or full phosphorylation, translocation and conformational changes in specific cytosolic proteins of the neutrophil, which then assemble to the enzyme *NADPH-oxidase* (*NOX*) [7, 19].

## 2.3 Chemoattractant-derived production of reactive oxygen species

Molecules identified as ROS are partially reduced metabolites of oxygen that possess strong oxidizing capabilities [19]. They are cytotoxic at high concentrations, for example, they oxidize cellular constituents and damage the DNA (e.g., see [2, 20, 21]). However, at low concentrations they serve different complex functions, for instance, as second messengers, involved in cell signaling, and as molecules specialized to damage

pathogens [22].

Most important ROS in neutrophil activity are *superoxide anion*  $O_2^{\cdot-}$ , *hydrogen peroxide*  $H_2O_2$  and *hypochlorous acid* HOCl (e.g., see [7, 23]). Those are generated by NOX both intra- and extracellularly, inside phagosomes and granuli. They can also be released from the cytoplasmic matrix.

Inside neutrophils, the active kinases phosphorylate specific cytosolic proteins, which bind to NOX, a transmembrane enzyme [24] (see Fig. 2). These processes can be interpreted as intermediate steps until a full activation of NOX; it is the *priming* phase [25]. During this phase, we say that neutrophils have a *primed state*. Usually, neutrophil's primed state differ from cell to cell [7, 19].

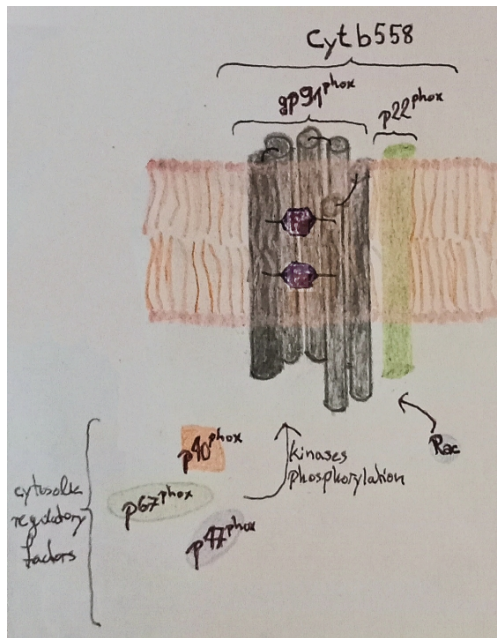


Figure 2: NADPH-oxidase at the membrane.<sup>2</sup>

There is no unique location for the enzyme NOX, thus 'membrane' can refer to diverse cell components: phagosome or also granuli membrane [26]. After assembly, NOX becomes active and converts oxygen into superoxide while oxidizing *nicotinamide adenine dinucleotide phosphate* (NADPH); superoxide is then quickly converted into peroxide (this is called *dismutation*) [7]. Neutrophils have an additional enzyme called *myeloperoxidase* (MPO) whose task is to produce HOCl from peroxide. MPO presence and activity is a unique feature of neutrophils [23, 27].

ROS contribute to damage bacteria, being HOCl the most damaging as it attacks any oxidizable group [27]. Furthermore, it is supposed that most of HOCl produced by MPO reacts with neutrophil proteins, damaging the neutrophil itself [28]. Peroxide is toxic only at higher concentrations and superoxide is mostly used to further reactions, however the latter might play a role in the migration of neutrophils. In case of higher

<sup>2</sup>This visual representation of the enzyme was inspired on the work of M. Mittal *et al.* [19]

concentrations, peroxide is degraded into water and oxygen via the enzyme catalase [29, 30].

Less important ROS are *hydroxyl radical*  $\cdot\text{OH}$  and *singlet oxygen*  $^1\text{O}_2$ . The first one is a product of the reaction between superoxide and peroxide or superoxide and HOCl. It is toxic to bacteria but, since it is highly reactive, its impact on the killing process is very low. Peroxide can also react with HOCl and release singlet oxygen, which has shown to have almost no relevance [23, 28].

Further biochemical products involving ROS are *reactive nitrogen species*, which might be also pathogen killers [23]. They are also out of the scope of this investigation.

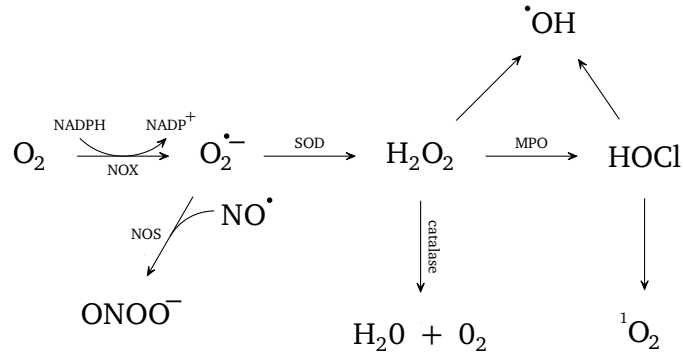


Figure 3: Description of the oxidative burst as a reaction network in which oxygen is the substrate [23].

## 2.4 Experimental setup



Figure 4: Observing area of the experiment.<sup>3</sup>

In collaboration with Dr. Gruber and the University Medical Center Regensburg, the behavior of neutrophils in inflammatory environments is investigated, in particular the attraction of the neutrophils by fMLP and the generation of ROS [9]. For this, neutrophils are placed on the right hand side of a squared experimental region filled with liquid culture medium (see Fig. 4). On the left hand side, the chemoattractant fMLP is concentrated. As time proceeds, fMLP diffuses through the domain, makes the diffusing neutrophils to move actively along its gradient and induces the production of ROS in neutrophils. The ROS molecules  $\cdot\text{OH}$  and HOCl are detected via the fluorescent dye *dihydrorhodamine-123 (DHR-123)*.

The experimental results showed that the higher the concentration of ROS, the slower the movement of neutrophils, thus giving a hint of an additional role of ROS in neutrophil chemotaxis.

Ongoing research of the biochemical processes reveals that the phenomenon of autophagy in PMNs is also strongly ROS-dependent. The exact biochemical mechanisms are still unknown but experimental results from Watson *et al.* [31] have shown that the rate of neutrophil apoptosis increases upon phagocytosis and is correlated to the ratio bacteria:neutrophil, which dictates the level of produced ROS [22].

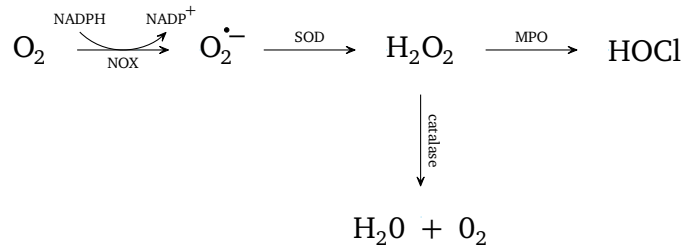
---

<sup>3</sup>This image was taken from the supplement material addressed in [10].

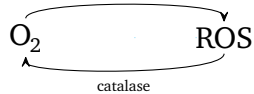
## 3 Mathematical modeling

### 3.1 Metabolic network for ROS

The goal of this investigation is to include ROS production and degradation in a chemotaxis model. From section 2.3, we will consider the most relevant substances only. Hence, we discard both hydroxyl radical and singlet oxygen from the network. Furthermore, we do not include reactive nitrogen species. These simplifications give the following network [7]:



Due to the fact that most of hydrogen peroxide is used to form hypochlorous acid [32], which was then detected by the fluorescent dye, and is also degraded via catalase, we further simplify the model to a single, generic ROS species:



This last reaction network is the basis for the model.

### 3.2 Mathematical model

To obtain a mathematical insight of the behavior of cells and ROS production, we suggest a model of partial differential equations to describe the evolution of the *cell density* ( $n$ ), *ROS concentration* ( $r$ ) and *chemoattractant concentration* ( $f$ ). The model, based on the famous chemotaxis model by Keller and Segel [3], considers a variable *chemotactic sensitivity* given by a function that depends on ROS concentration ( $\chi(r)$ ). Doing so, we can analyze the impact of the production of ROS on the movement of cells. The model proposed by Höfer *et al.* [33, 34], follows a similar approach by introducing a new function that regulates the behavior of the chemotactic sensitivity, and thus it gives us a hint for the following formulation.

Let  $n$ ,  $r$  and  $f$  be defined as functions of time and space:

$$n = n(t, x), \quad (1)$$

$$r = r(t, x), \quad (2)$$

$$f = f(t, x). \quad (3)$$

As described in section 2.3, oxygen is crucial for the oxidative burst [11]. Therefore, in the following we denote *oxygen concentration* by

$$w = w(t, x). \quad (4)$$

a) **Cell density:**

For simplicity, we consider a homogeneous population of neutrophils, meaning that all cells have the same priming status. The flux of the cell density is given by:

$$J_n := \underbrace{-D_n \nabla n}_{\text{diffusion}} + \underbrace{\chi(r)n \nabla f}_{\text{chemotaxis}}. \quad (5)$$

It consists of a diffusive term and a chemotactic term. Here,  $D_n > 0$  is the *diffusion constant* and  $\chi$  denotes the chemotactic sensitivity, which depends on ROS concentration as follows:

$$\chi(r) = \chi_0 \frac{R_1}{R_2 + r}. \quad (6)$$

The constant  $\chi_0$  is a positive real number and serves as the chemotactic sensitivity in case no ROS were produced by the cell. We assume that there is a threshold relating ROS amount within a cell and its movement, which is determined by the positive parameters  $R_1$  and  $R_2$ , particularly by the proportion  $\frac{R_1}{R_2}$ .

From section 2.4 we know that ROS plays a role in the death of PMNs. Thus, we consider the cell death by *degradation function*  $\lambda(r)$ , with  $\lambda$  a non-negative function. Hence, we have the following equation for the evolution of the cell density:

$$\partial_t n = -\nabla \cdot J_n - \lambda(r)n. \quad (7)$$

b) **Chemoattractant concentration:**

The chemoattractant is consumed [17] with rate constant  $\beta \geq 0$  and also diffusion takes place. The equation is given by:

$$\partial_t f = \underbrace{D_f \Delta f}_{\text{diffusion}} - \underbrace{\beta n \frac{V_{\max}}{K_f + f} f}_{\text{consumption}}. \quad (8)$$

We have the *chemoattractant's diffusion constant*  $D_f > 0$  and an interaction term between chemoattractant and cell. The constant  $K_f > 0$  is based on the *binding affinity* constant, which represents the usual interaction between FPRs and the correspondent ligand, here fMLP. Furthermore, these receptors have a saturation threshold, the *maximum binding capacity*  $V_{\max}$ , that restricts how much fMLP can be sensed by the cell [35, 36]. That means, a neutrophil will not react always to the chemoattractant, regardless of how much chemoattractant concentration is present in the environment. This saturation constant has a positive value.

c) **ROS concentration:**

The production of ROS is considered to occur only intracellularly (i.e. within phagosomes and granuli) and is modeled following *Michaelis-Menten dynamics*. Note that ROS are not only being produced by the cells, but also transported with

them. However, we assume that the time-scale of their production is much faster than the spatial movement. Therefore, we will neglect the diffusive contribution. As a consequence, for the dynamic of ROS concentration we have only an ODE, namely

$$\partial_t r = h(n, f, r, w), \quad (9)$$

where

$$h(n, f, r, w) = v_1(w)\eta(f)\rho(n) - v_2(r). \quad (10)$$

We consider a fictive enzyme that converts oxygen to ROS with velocity

$$v_1 = v_1(w).$$

This velocity is defined as

$$v_1(w) := \frac{V_{M,1}w}{K_w + w}, \quad (11)$$

where  $V_{M,1}$  is the *maximal production rate* and  $K_w$  is the so called *Michaelis constant*. The function  $\eta(f)$  models the dependence of the oxidative burst under chemoattractant's presence, which triggers it. We also have a function  $\rho(n)$  that relates ROS generation with cell density. To do that, we define  $\rho$  in the following way:

$$\rho(n) := \frac{V_{M,2}n}{K_n + n}. \quad (12)$$

Last but not least, *catalase's velocity* is denoted by

$$v_2 = v_2(r).$$

For the formulation of the full mathematical model describing the relevant processes in the experiment, let  $\Omega$  be a bounded, connected subset of  $\mathbb{R}^2$ , for instance,

$$\Omega = (-L, L) \times (0, h); \quad L, h > 0,$$

with boundary

$$\partial\Omega = \Gamma_1 \cup \Gamma_2 \cup \Gamma_3,$$

where

$$\begin{aligned} \Gamma_1 &:= \{(-L, x_2) : 0 < x_2 < h\}, \\ \Gamma_2 &:= \{(L, x_2) : 0 < x_2 < h\}, \\ \Gamma_3 &:= \partial\Omega \setminus (\Gamma_1 \cup \Gamma_2) = \{(x_1, x_2) : x_1 \in [-L, L], x_2 \in \{0, h\}\}. \end{aligned}$$

Let  $T > 0$  a finite real number and define the time interval  $I$  for the process by

$$I := (0, T).$$

This last assumption is biologically sensible as the cellular processes do not last for ever.

We look for a solution  $(n, f, r)$  of the following system:

$$\partial_t n(t, x) = \nabla \cdot (D_n \nabla n(t, x) - \chi(r)n(t, x)\nabla f(t, x)) - \lambda(r)n(t, x), \quad (13)$$

$$\partial_t f(t, x) = D_f \Delta f(t, x) - \beta n \frac{V_{\max}}{K_f + f} f(t, x), \quad (14)$$

$$\partial_t r(t, x) = \frac{V_{M,1}w}{K_w + w} \eta(f)\rho(n) - \nu_2(r), \quad (15)$$

with  $t \in I$  and  $x = (x_1, x_2) \in \Omega$ , together with the following boundary conditions:

$$(D_n \nabla n(t, x) - \alpha \chi(r)n \nabla f) \cdot \nu(x) = 0, \quad \text{at } \partial\Omega, \quad (16)$$

$$f(t, x) = f_1(x), \quad \text{at } \Gamma_1, \quad (17)$$

$$f(t, x) = f_2(x), \quad \text{at } \Gamma_2, \quad (18)$$

$$\nabla f(t, x) \cdot \nu(x) = 0, \quad \text{at } \Gamma_3. \quad (19)$$

Here,  $\nu(x)$  is the unit normal vector at  $x \in \partial\Omega$  pointing outwards. The constant  $\alpha \in [0, 1]$  is a *boundary parameter* and regulates how does the flux go through the boundary. If  $\alpha = 1$ , we obtain an impermeable boundary. In this work, we consider  $\alpha = 0$ , i.e., homogeneous Neumann boundary conditions for the cell density  $n$ . For the chemoattractant, we set Dirichlet boundary conditions at  $\Gamma_1$  and  $\Gamma_2$ , and define  $f_1(x)$ ,  $f_2(x)$  to be functions depending only on space.

The initial values are

$$n(0, x) = n_0(x), \quad (20)$$

$$f(0, x) = f_0(x), \quad (21)$$

$$r(0, x) = r_0(x). \quad (22)$$

In the following, this mathematical model (13)-(22) is used for the investigation of the biochemical processes by numerical simulations.



## 4 Numerical results

The simulation of the model (13)-(22) was done with MATLAB<sup>®</sup> by MathWorks<sup>®</sup>, in particular with the Partial Differential Equation Toolbox<sup>™</sup>. This package solves systems of partial differential equations (PDEs) numerically, implementing the finite element method [37]. Given a domain  $\Omega$ , a time interval  $I$  and a time-step size  $\Delta t$ , the PDE system

$$\mathbf{D} \frac{\partial \vec{u}}{\partial t} - \nabla \cdot (\mathbf{C} \otimes \nabla \vec{u}) + \mathbf{A} \vec{u} = \vec{f}$$

is solved for  $\vec{u} = (n, f, r)^T$ . In the discretized setting, the coefficients  $\mathbf{D}, \mathbf{A}$  are  $3 \times 3$  matrices,  $\mathbf{C}$  is a  $3 \times 3 \times 2 \times 2$  tensor and  $\vec{f}$  a vector. All of them are allowed to depend of time, space,  $\vec{u}$  itself and even its gradient. The finite element method uses Lagrange quadratic polynomial interpolation on triangular elements. This means, the nodes are at the vertices and also at the midpoints of the edges. The final result can be plotted, thus obtaining a stream of visualizations and a discrete evolution of the solution.

For the numerical simulations, we have considered the following setting (see Fig. 5): let  $L = 1$  and  $h = 0.1$  such that

$$\Omega = (-1, 1) \times (0, 0.1),$$

and the boundary  $\partial\Omega$  is given by

$$\begin{aligned}\Gamma_1 &= \{(-1, x_2) : 0 \leq x_2 \leq 0.1\}, \\ \Gamma_2 &= \{(1, x_2) : 0 \leq x_2 \leq 0.1\}, \\ \Gamma_3 &= \{(x_1, x_2) : x_1 \in (-1, 1), x_2 \in \{0, 0.1\}\}.\end{aligned}$$

We consider the time interval  $I = (0, 200)$  and the time step is chosen as  $\Delta t = 0.1$ . The domain was discretized in 100 triangular elements with a total of 253 nodes. The iterative discrete solution was computed by an internal ODE solver that relies on Numerical Differentiation Formulas [38].

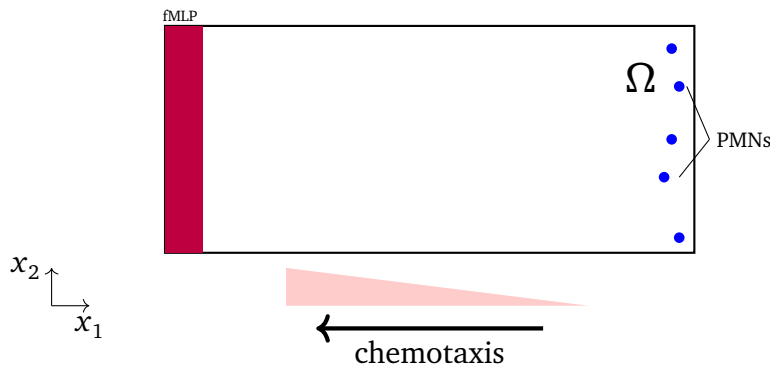


Figure 5: Sketch of the simulation setting.

Initially, the cells are concentrated inside the region  $(0.7, 0.9) \times (0, 0.1) \subset \Omega$  (see Fig. 6), thus the initial value

$$n_0(x_1, x_2) = \begin{cases} 18, & \text{if } 0.7 < x_1 < 0.9, \\ 0, & \text{else.} \end{cases}$$

ROS concentration has the following initial value  $r_0(x) \equiv 0$ . Furthermore, the function  $\eta(f)$  in the production of chemoattractant is given by  $\eta(f) \equiv f$ . All the remaining parameters and functions in the equations, initial values and boundary conditions are given in Table 1.

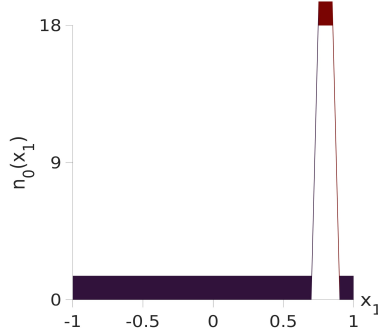


Figure 6: Initial value  $n_0$

Equation	Parameter or function	Value
(4)	$w(t, x)$	20
(5)	$D_n$	$2.5 \times 10^{-3}$
(6)	$\chi_0$	10
(6)	$R_1$	0.1
(6)	$R_2$	1
(7)	$\lambda(r)$	0
(8)	$D_f$	$1 \times 10^{-5}$
(8)	$\beta$	0.35
(8)	$V_{max}$	$1 \times 10^{-5}$
(8)	$K_f$	$1 \times 10^{-3}$
(10)	$v_2(r)$	$0.35r$
(11)	$V_{M,1}$	10
(11)	$K_w$	1
(12)	$V_{M,2}$	1
(12)	$K_n$	10
(17)	$f_1(x)$	0.01
(18)	$f_2(x)$	0.001

Table 1: Parameter values used in the presented numerical simulations.

We performed our numerical simulations for two different scenarios.

## 4.1 Simulation with given chemoattractant concentration

For this computational scenario we consider the chemoattractant to be given as the time-independent, affine linear function

$$f(t, x) := -0.0045x_1 + 0.0055.$$

This function, shown in Fig. 7, is chosen such that the boundary values coincide with the boundary conditions imposed in the second scenario, namely

$$\begin{aligned} f_1(-1) &= 0.01, \\ f_2(1) &= 0.001. \end{aligned}$$

We neglect cellular and ROS degradation by setting

$$\begin{aligned} \lambda(r) &\equiv 0, \\ \nu_2(r) &\equiv 0. \end{aligned}$$

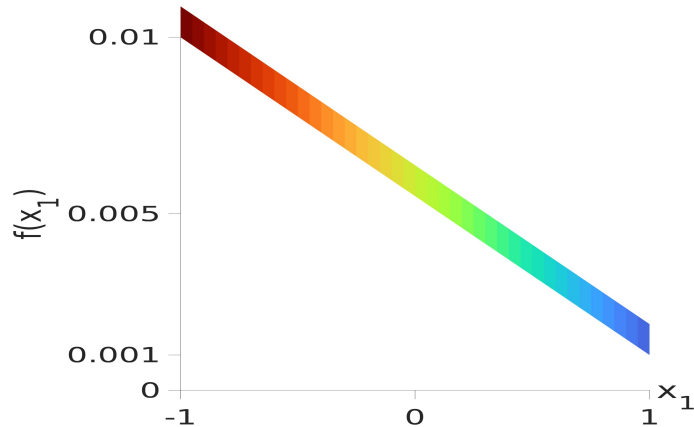


Figure 7: Given chemoattractant concentration

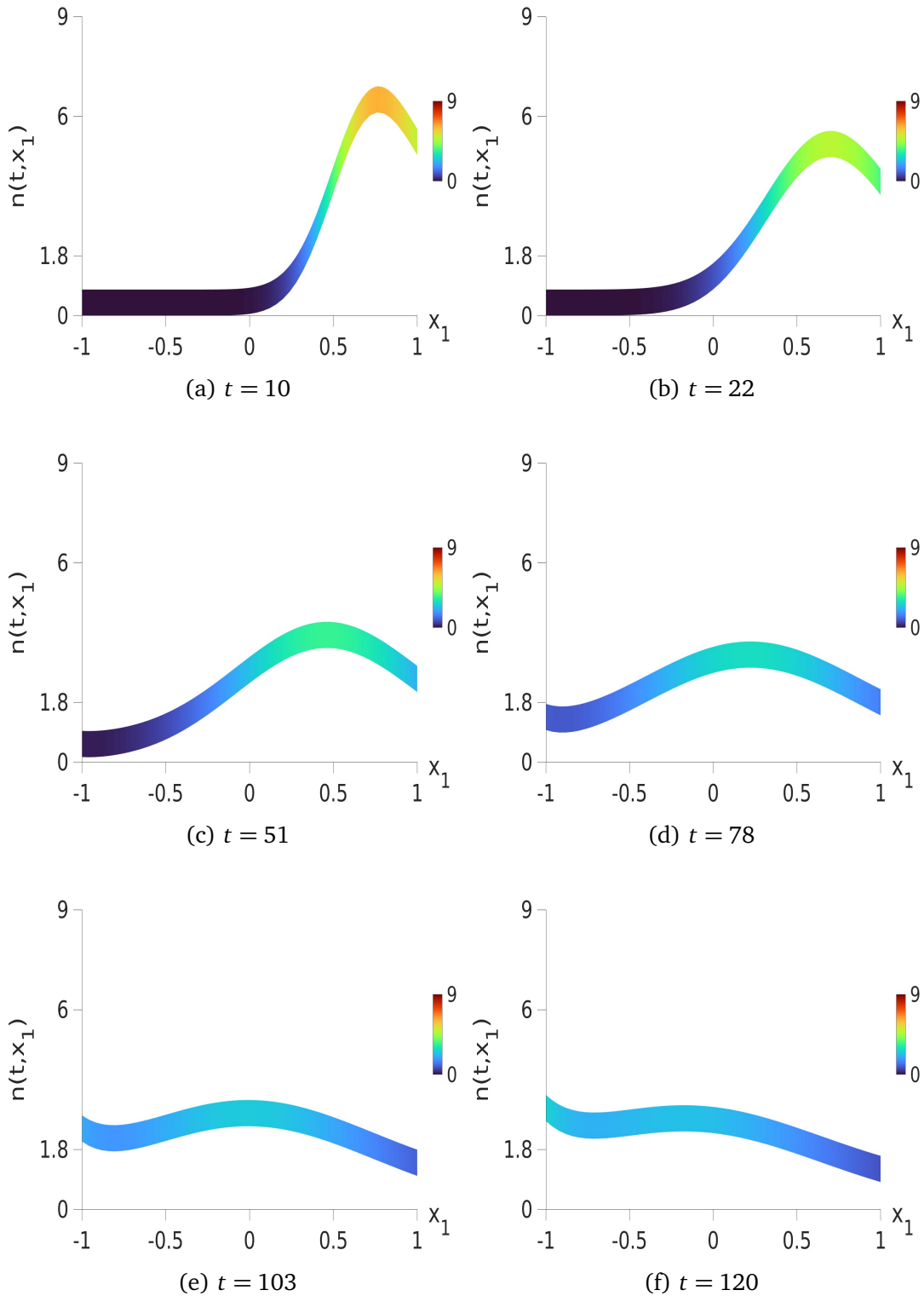


Figure 8: Spatial distribution of the cell density  $n$  with ROS-independent chemosensitivity ( $\chi(r) = \chi_0 \frac{R_1}{R_2}$ ) at the indicated time values  $t$ .

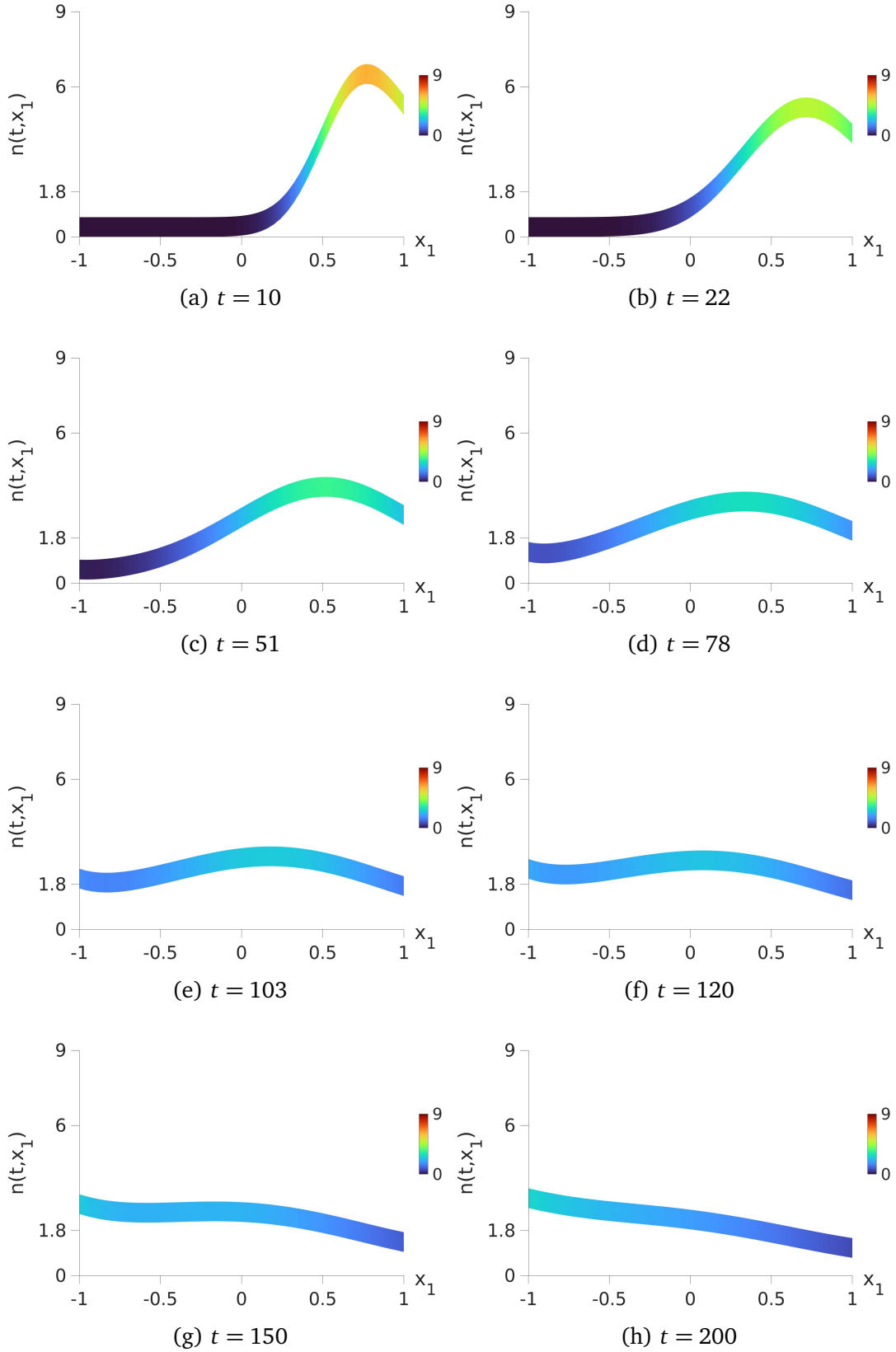


Figure 9: Profiles (a)-(h) show the spatial distribution of the cell density  $n$  with variable chemosensitivity ( $\chi(r) = \chi_0 \frac{R_1}{R_2 + r}$ ) for the indicated time values  $t$ .

The first simulation results, in Fig. 8, are performed for a ROS-independent chemosensitivity  $\chi(r) = \chi_0 \frac{R_1}{R_2}$ . We see that the cells move to the left side of the domain, in direction of the chemoattractant gradient. In Fig. 9, we observe an accumulation of cells in the neighborhood of the boundary. This effect results partly from the homogeneous Neumann boundary conditions.

In Fig. 9, the results for a ROS-dependent chemosensitivity  $\chi(r) = \chi_0 \frac{R_1}{R_2+r}$  have been performed. Again, the movement of cells in direction of chemoattractant gradient can be observed. Comparing the results in Fig. 8 and Fig. 9, the peaks of the waves at times  $t = 51$  and  $t = 78$  lie a bit behind in the second case. This shows that with a ROS-dependent chemosensitivity the movement is slightly restricted. To quantify this aspect, the centers of mass have ben computed and can be compared in Fig. 10.

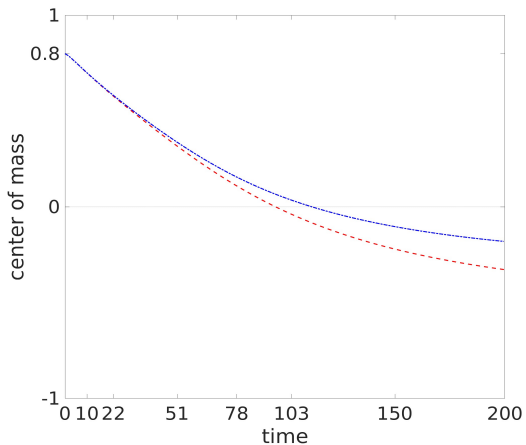


Figure 10: Evolution in time in the  $x_1$ -direction of the center of mass of the cell density. The red line shows the ROS-independent case whereas the blue line results from the ROS-dependent chemosensitivity.

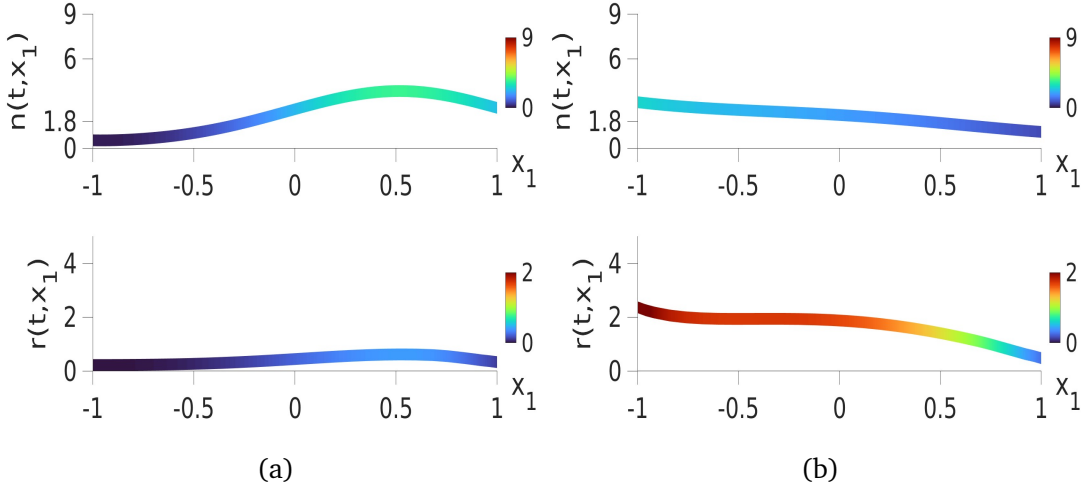


Figure 11: Cell density  $n$  and ROS concentration  $r$  at time values (a)  $t = 51$  and (b)  $t = 200$ .

In Fig. 11 the evolution of the cell density and ROS concentration are plotted. At  $t = 51$ , see Fig. 11a, both profiles, cell density and ROS production, have a similar shape. We can notice that ROS concentration levels are higher there, where the cell density has its peak and this is in accordance with the fact that ROS is produced inside the cells. At  $t = 200$ , see Fig. 11b, the cell density is almost flattened. We can observe increasing ROS concentration levels in the left part of the domain, where the chemoattractant has higher concentration.

Recall that in this setting we considered a fixed chemoattractant gradient. Furthermore, ROS degradation is not included. In the following section we will consider a more realistic situation.

## 4.2 Simulation with variable chemoattractant concentration

The second computational scenario considers the full PDE model (13)-(22). In this case, the chemoattractant is the solution of a reaction-diffusion equation with diffusion parameter  $D_f = 1 \times 10^{-5}$  and initial value

$$f_0(x) = -0.002x_1 + 0.003.$$

All other parameters of the model can be found in Table 1.

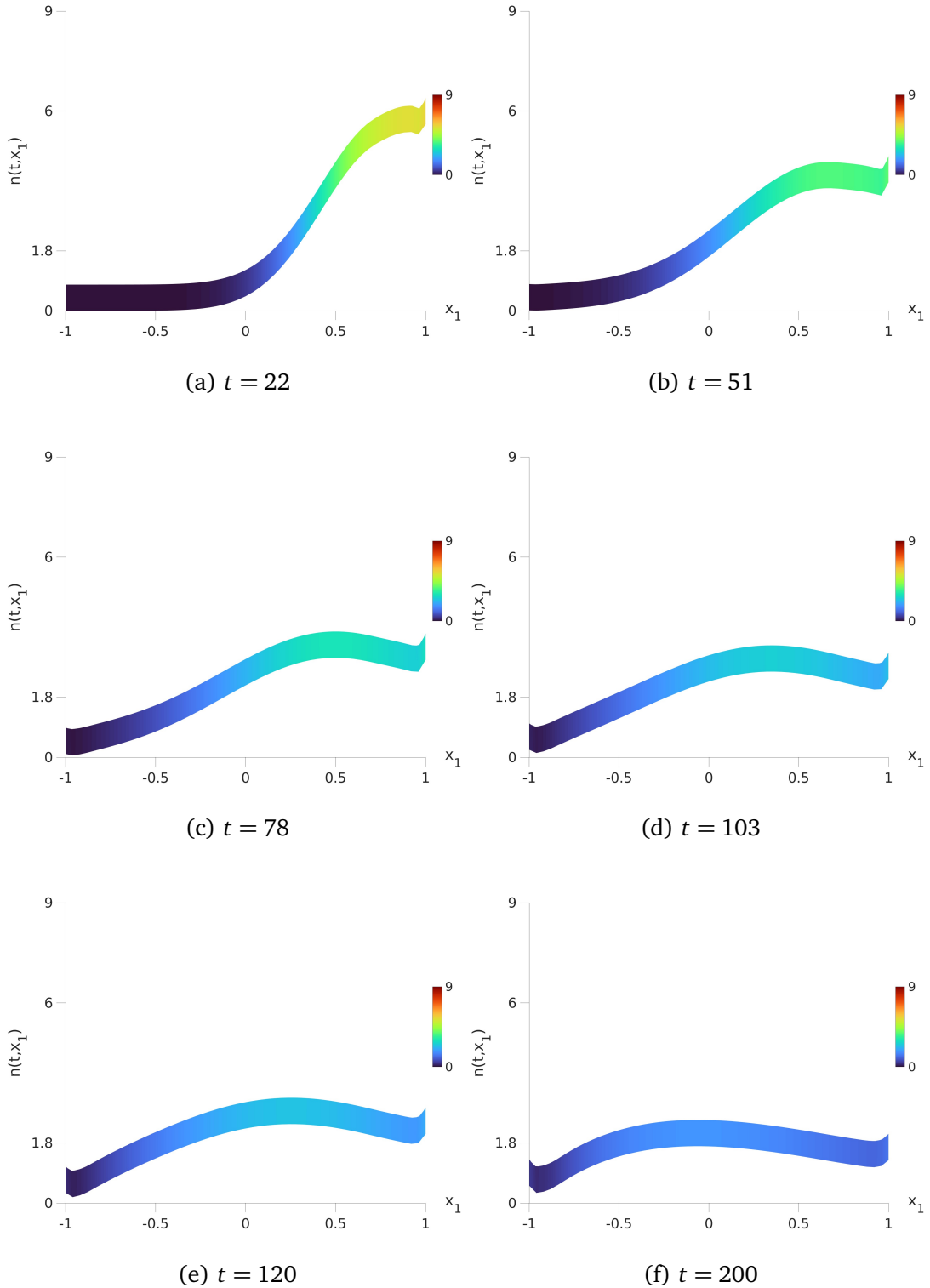


Figure 12: Spacial distribution of the cell density  $n$  with variable chemosensitivity and chemoattractant for the indicated time values  $t$ .

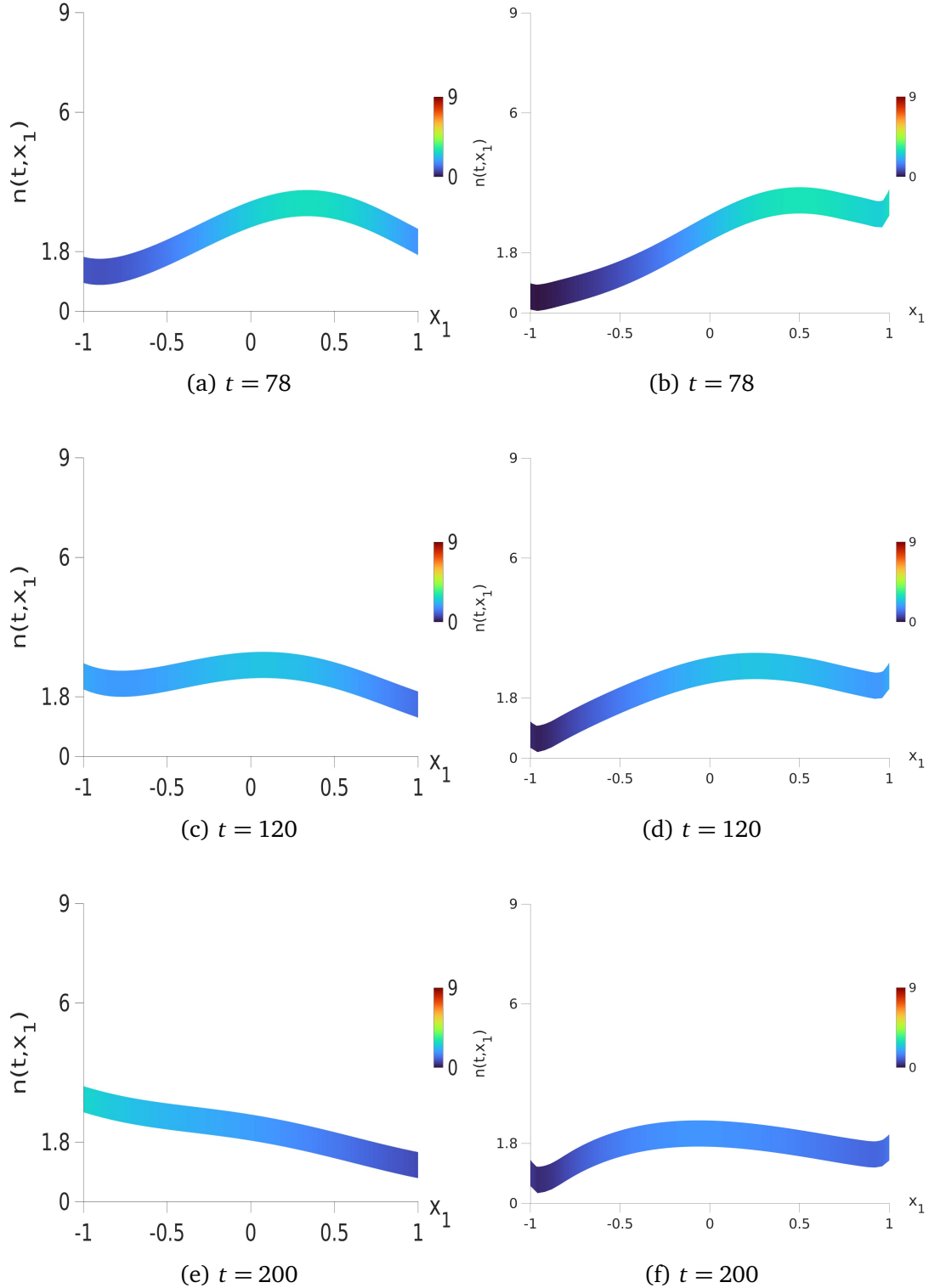


Figure 13: Comparison of the evolution in time of both scenarios. At the left, the first scenario with fix chemoattractant is shown; at the right, the current scenario with variable gradient.

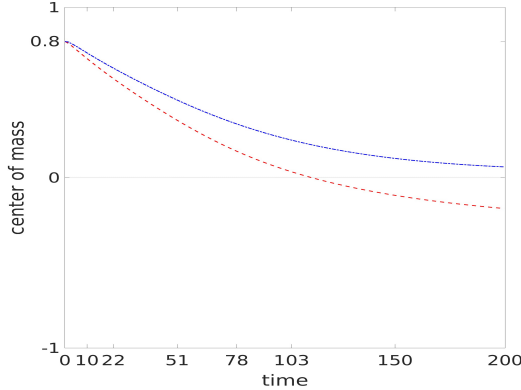


Figure 14: Evolution in time in the  $x_1$ -direction of the center of mass of the cell density. Both cases refer to ROS-dependent chemosensitivity. The red line shows the evolution for the first scenario and the blue line for this second scenario.

Analogous to the first scenario, in Fig. 12 we can see that the cells move to the left part of the domain. We see in Fig. 13, for the first scenario, that the density at the left boundary reaches a value notoriously higher than 10% of the initial value  $n_0$  (see Fig. 13c) and in the second scenario it remains considerably smaller. We know already that chemotaxis is triggered by an increasing gradient of fMLP and that the higher the chemoattractant concentration gets, the larger is the production of ROS inside cells. In Fig. 10 we verify the slowing down effect of ROS in the movement and now we can establish that higher levels of ROS might even counteract the attraction, allowing a fewer amount of cells to reach the left boundary.

We observe a similarity in the slowed down movement. An important difference is the displacement after a similar time. We also observe, in Fig. 14, that in the second scenario the centers of mass do not move as much as in the first scenario, lying behind those.

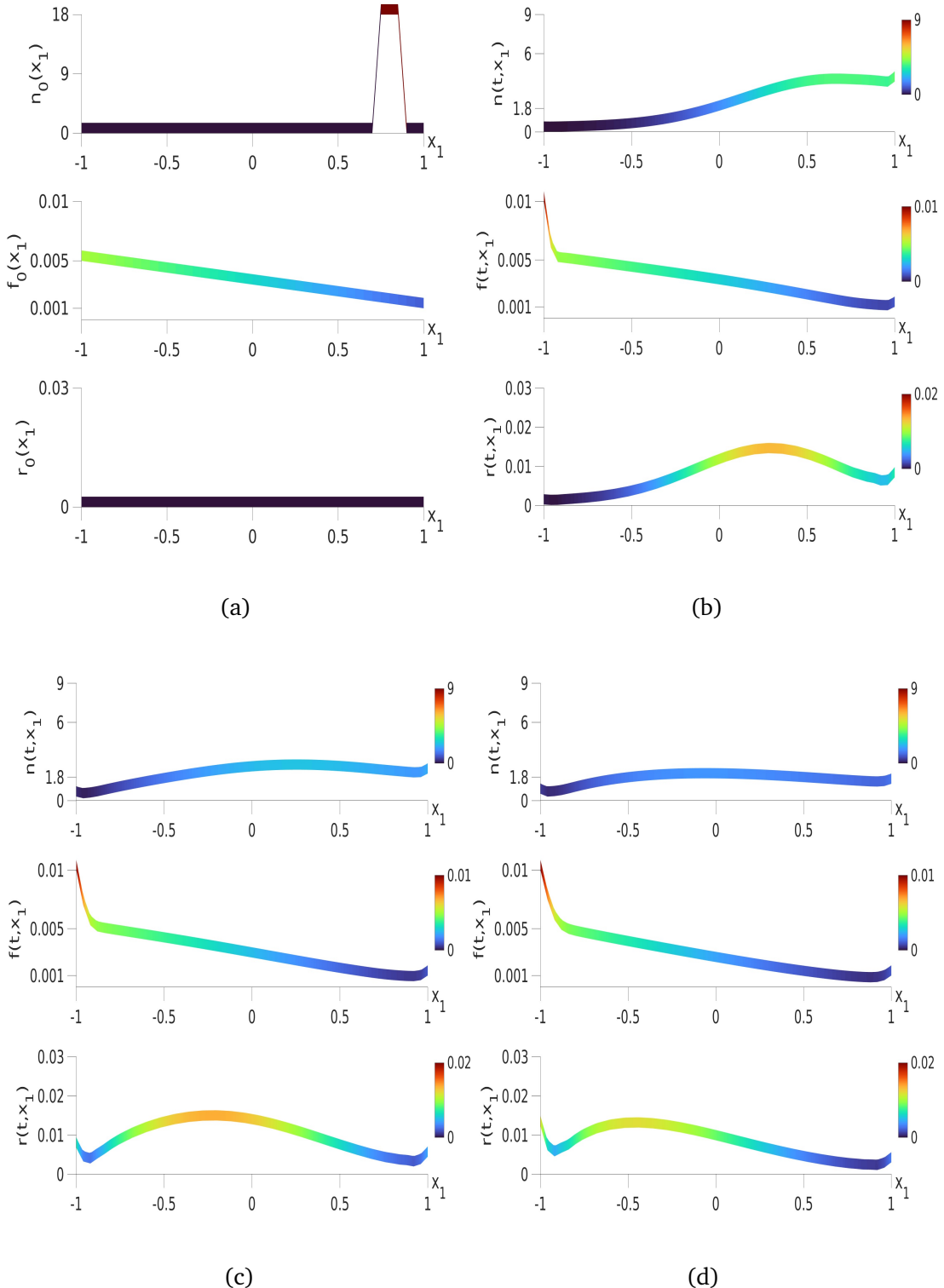


Figure 15: In (a) the initial values  $n_0$ ,  $f_0$  and  $r_0$  can be seen. In (b)-(d), cell density  $n$ , fMLP concentration  $f$  and ROS concentration  $r$  are depicted for time values  $t = 51$ ,  $t = 120$  and  $t = 200$  respectively.

In Fig. 15 we observe the three variables simultaneously. We compare their initial values (see Fig. 15a) with the resulting distribution within the domain for three different time values. In Fig. 15d, from the z-axis we see that ROS concentration levels are less than 10% of the highest values depicted in Fig. 11b. Even with this lower production, in terms of concentration levels, they have a stronger effect on cell movement, restraining it and slowing it down faster (see Fig. 13). Notice also that fMLP concentration builds an increasing gradient at both boundaries with respect to the middle part of the domain. Therefore, we have increasing values for  $n$  and  $r$  near both sides. These visualizations helps us to analyze better the interplay of all variables. Cells move due attraction and ROS starts to be produced (see Fig. 15b). There, where cell density has higher values above 10% of  $n_0$ , ROS production keeps increasing but it decays quickly for lower ones despite fMLP concentration being much higher than in the middle of the domain (see Fig. 15c). At the end, ROS degradation can be noticed as the whole profile sinks a bit to the bottom of the graphic. Nevertheless, the effect on the chemotaxis can still be identified due to cells being restricted to move towards the chemoattractant as fast as the beginning.

## 5 Conclusion

In this thesis, we propose a chemotaxis model for neutrophils in inflammatory environments motivated on the experiment results presented in [9]. The novel aspect concerning this model, consists of the fact that it includes an additional variable in comparison to the model in [3], namely the concentration of ROS, which is a consequence of cellular activity under the influence of the chemoattractant and has an impact on the motility of neutrophils.

The resulting model is a fully non-linearly coupled PDE system. Using numerical tools, we performed computational simulations in order to determine the evolution in time and space of those variables. Finally, with the help of the model, we can recover qualitatively the experimental features, in particular that ROS play an important role in neutrophil motility, see, e.g., Fig. 14. One important aspect is the analytic investigation of the well-posedness of this model and a starting point can be found in the procedures mentioned in [4].

As described in [10], additional processes could be taken into account to obtain a more realistic, complete model, for example, the presence of the different priming phases within a cell population or neutrophil's death induced by ROS-mediated suicidal NETosis [7, 14]. Besides these mentioned processes, there are even more pathways and mechanisms that occur simultaneously. With the help of such a mathematical model, we can describe that complex interplay more precisely and, therefore, clarify how neutrophils behave when bacterial infection takes place. That knowledge is relevant, e.g., for the development of therapeutic strategies to prevent autoimmune activity which results from persistent neutrophil functionality [13].

## References

- <sup>1</sup>C. W. Baldridge and R. W. Gerard, “The extra respiration of phagocytosis”, *American Journal of Physiology* **103**, 235–236 (1933).
- <sup>2</sup>L. Fialkow, Y. Wang, and G. P. Downey, “Reactive oxygen and nitrogen species as signaling molecules regulating neutrophil function”, *Free Radical Biology & Medicine* **42**, 153–164 (2007).
- <sup>3</sup>E. F. Keller and L. A. Segel, “The initiation of slime mold aggregation viewed as an instability”, *Journal of Theoretical Biology* **26**, 399–415 (1970).
- <sup>4</sup>A. Kettemann and M. Neuss-Radu, “Derivation and analysis of a system modeling the chemotactic movement of hematopoietic stem cells”, *Journal of Mathematical Biology* **56**, 579–610 (2008).
- <sup>5</sup>M. Gabel, “Ein Chemotaxis-Modell mit Adaption”, Cand. thesis (Ruprecht-Karls-Universität Heidelberg, 2012).
- <sup>6</sup>L. Michaelis and M. L. Menten, “Die Kinetik der Invertinwirkung”, *Biochemische Zeitschrift* **79**, 333–369 (1913).
- <sup>7</sup>J. El-Benna, M. Hurtado-Nedelec, V. Marzaioli, J.-C. Marie, M.-A. Gougerot-Pocidalo, and P. M.-C. Dang, “Priming of the neutrophil respiratory burst: role in host defense and inflammation”, *Immunological Reviews* **273**, 180–193 (2016).
- <sup>8</sup>R. C. Schugart, A. Friedman, R. Zhao, and C. K. Sen, “Wound angiogenesis as a function of tissue oxygen tension: a mathematical model”, *Proceedings of the National Academy of Sciences of the United States of America* **105**, 2628–2633 (2008).
- <sup>9</sup>D. Pai, M. Gruber, S.-M. Pfaehler, A. Bredthauer, K. Lehle, and B. Trabold, “Polymorphonuclear Cell Chemotaxis and Suicidal NETosis: simultaneous Observation Using fMLP, PMA, H7 and Live Cell Imaging”, *Journal of Immunology Research* **2020**, 1415947 (2020).
- <sup>10</sup>R. F. Kraus and M. A. Gruber, “Neutrophils—From bone Marrow to First-Line Defense of the Innate Immune System”, *Frontiers in Immunology* **12**, 767175 (2021).
- <sup>11</sup>A. W. Segal and S. B. Coade, “Kinetics of oxygen consumption by in phagocytosing”, *Biochemical and Biophysical Research Communications* **84**, 611–617 (1978).
- <sup>12</sup>D. V. Zhelev, A. M. Alteraifi, and D. Chodniewicz, “Controlled Pseudopod Extension of Human Neutrophils Stimulated with Different Chemoattractants”, *Biophysical Journal* **87**, 688–695 (2004).
- <sup>13</sup>M. Metzemaekers, M. Gouwy, and P. Proost, “Neutrophil chemoattractant receptors in health and disease: double-edged swords”, *Cellular & Molecular Immunology* **17**, 433–450 (2020).
- <sup>14</sup>W. Stoiber, A. Obermayer, P. Steinbacher, and W.-D. Krautgartner, “The Role of Reactive Oxygen Species (ROS) in the Formation of Extracellular Traps (ETs) in Humans”, *Biomolecules* **5**, 702–723 (2015).

- <sup>15</sup>R. D. Ye, F. Boulay, J. M. Wang, C. Dahlgren, C. Gerard, M. Parmentier, C. N. Serhan, and P. Murphy, “Nomenclature for the Formyl Peptide Receptor (FPR) Family”, *Pharmacological Reviews* **61**, 119–161 (2009).
- <sup>16</sup>C. Koo, R. J. Lefkowitz, and R. Snyderman, “The oligopeptide chemotactic factor receptor on human polymorphonuclear leukocyte membranes exists in two affinity states”, *Biochemical and Biophysical Research Communications* **106**, 442–449 (1982).
- <sup>17</sup>V. V. Gurevich and E. V. Gurevich, “GPCR Signaling Regulation: The Role of GRKs and Arrestins”, *Frontiers in Pharmacology* **10**, 125 (2019).
- <sup>18</sup>K. Chen, Z. Bao, W. Gong, P. Tang, T. Yoshimura, and J. M. Wang, “Regulation of inflammation by members of the formyl-peptide receptor family”, *Journal of Autoimmunity* **85**, 64–77 (2017).
- <sup>19</sup>M. Mittal, M. R. Siddiqui, K. Tran, S. Reddy, and A. Malik, “Reactive Oxygen Species in Inflammation and Tissue Injury”, *Antioxidants & Redox Signaling* **20**, 1126–1167 (2014).
- <sup>20</sup>G. Brandi, M. Fiorani, C. Pierotti, A. Albano, F. Cattabeni, and C. Orazio, “Morphological Changes in *Escherichia coli* Cells Exposed to Low or High Concentrations of Hydrogen Peroxide”, *Microbiology and Immunology* **33**, 991–1000 (1989).
- <sup>21</sup>S. M. McKenna and K. J. A. Davies, “The inhibition of bacterial growth by hypochlorous acid. Possible role in the bactericidal activity of phagocytes”, *Biochemical Journal* **254**, 685–692 (1988).
- <sup>22</sup>S. Dupré-Crochet, M. Erard, and O. Nüsse, “ROS production in phagocytes: why, when and where?”, *Journal of Leukocyte Biology* **94**, 657–670 (2013).
- <sup>23</sup>M. B. Hampton, A. J. Kettle, and C. C. Winterbourn, “Inside the Neutrophil Phagosome: Oxidants, Myeloperoxidase and Bacterial Killing”, *Blood* **92**, 3007–3017 (1998).
- <sup>24</sup>A. R. Cross and A. W. Segal, “The NADPH oxidase of professional phagocytes—prototype of the NOX electron transport chain systems”, *Biochimica et Biophysica Acta* **1657**, 1–22 (2004).
- <sup>25</sup>L. C. McPhail, P. S. Shirley, C. C. Clayton, and R. Snyderman, “Activation of the Respiratory Burst Enzyme from Human Neutrophils in a Cell-free System”, *Journal of Clinical Investigation* **75**, 1735–1739 (1985).
- <sup>26</sup>A. Karlsson, J. Nixon, and L. McPhail, “Phorbol myristate acetate induces neutrophil NADPH-oxidase activity by two separate signal transduction pathways: dependent or independent of phosphatidylinositol 3-kinase”, *Journal of Leukocyte Biology* **67**, 396–404 (2000).
- <sup>27</sup>A. J. Kettle and C. C. Winterbourn, “Myeloperoxidase: a key regulator of neutrophil oxidant production”, *Redox Report* **3**, 3–15 (1997).
- <sup>28</sup>A. J. Kettle and C. C. Winterbourn, “A Kinetic Analysis of the Catalase Activity of Myeloperoxidase”, *Biochemistry* **40**, 10204–10212 (2001).

- <sup>29</sup>N. J. Adimora, D. P. Jones, and M. L. Kemp, “A Model of Redox Kinetics Implicates the Thiol Proteome in Cellular Hydrogen Peroxide Responses”, *Antioxidants & Redox Signaling* **13**, 731–743 (2010).
- <sup>30</sup>C. Komalapriya, D. Kaloriti, A. T. Tillmann, Z. Yin, C. Herrero-de Dios, M. D. Jacobsen, R. C. Belmonte, G. Cameron, K. Haynes, C. Grebogi, A. P. S. de Moura, N. A. R. Gow, M. Thiel, J. Quinn, A. J. P. Brown, and M. C. Romano, “Integrative Model of Oxidative Stress Adaptation in the Fungal Pathogen *Candida albicans*”, *PLOS One* **10**, 0137750 (2015).
- <sup>31</sup>R. W. G. Watson, H. P. Redmond, J. H. Wang, C. Condron, and D. Bouchier-Hayes, “Neutrophils Undergo Apoptosis Following Ingestion of *Escherichia coli*”, *The Journal of Immunology* **156**, 3986–3992 (1996).
- <sup>32</sup>C. C. Winterbourn, M. B. Hampton, J. H. Livesey, and A. J. Kettle, “Modeling the Reactions of Superoxide and Myeloperoxidase in the Neutrophil Phagosome”, *Journal of Biological Chemistry* **281**, 39860–39869 (2006).
- <sup>33</sup>T. Höfer, P. K Maini, J. A. Sherratt, M. A. J. Chaplain, P. Chauvet, D. Metevier, P. C. Montes, and J. D. Murray, “A Resolution of the Chemotactic Wave Paradox”, *Applied Mathematics Letters* **7**, 1–5 (1993).
- <sup>34</sup>T. Höfer, P. K. Maini, J. A. Sherratt, M. A. J. Chaplain, and J. D. Murray, “Resolving the chemotactic wave paradox: a mathematical model for chemotaxis of *Dictyostelium amoebae*”, *Journal of Biological Systems* **3**, 967–973 (1995).
- <sup>35</sup>A. Lala, H. T. Sojar, and E. De Nardin, “Expression and Purification of Recombinant Human N-Formyl-L-leucyl-L-phenylalanine (FMLP) Receptor”, *Biochemical Pharmacology* **54**, 381–390 (1997).
- <sup>36</sup>E. C. Hulme and M. A. Trevethick, “Ligand binding assays at equilibrium: validation and interpretation”, *British Journal of Pharmacology* **161**, 1219–1237 (2010).
- <sup>37</sup>The MathWorks, Inc., *Partial Differential Equation Toolbox™ User’s Guide*, version R2022a (2022).
- <sup>38</sup>L. F. Shampine and M. W. Reichelt, “The MATLAB ODE Suite”, *SIAM Journal on Scientific Computing* **18**, 1–22 (1997).

## **Erklärung**

Hiermit versichere ich, dass ich die vorliegende Arbeit selbstständig verfasst und keine anderen als die angegebenen Quellen und Hilfsmittel benutzt habe, dass alle Stellen der Arbeit, die wörtlich oder sinngemäß aus anderen Quellen übernommen wurden, als solche kenntlich gemacht sind und dass die Arbeit in gleicher oder ähnlicher Form noch keiner Prüfungsbehörde vorgelegt wurde.

Erlangen, den September 28, 2022